

# A Study on Aluminum-Based Lightweight Entropic Alloys with High Strength at Elevated Temperature

Liyang Cui<sup>1</sup> (✉), Zhan Zhang<sup>1</sup>, Dilip K. Sarkar<sup>1</sup>, Duygu Kocaefer<sup>1</sup>,  
and X. -Grant Chen<sup>1</sup>

<sup>1</sup> Department of Applied Science, University of Quebec at Chicoutimi, QC, Canada  
[liyang.cuil@uqac.ca](mailto:liyang.cuil@uqac.ca)

**Abstract.** Entropic alloys are a category of emerging advanced materials derived from the novel design concept of high-entropy alloys, which are also known as multicomponent alloys or complex concentrated alloys. In this study, two Al-based lightweight entropic alloys,  $\text{Al}_{74}\text{Cu}_{16}\text{Cr}_1\text{Zn}_7\text{Mg}_2$  and  $\text{Al}_{78}\text{Cu}_{18}\text{Cr}_2\text{Zn}_1\text{V}_1$ , were designed using a strategy based on physical thermodynamic parameters and Thermo-Calc simulations. The microstructures of the as-cast alloys revealed a multiphase feature, including fcc-Al solid solution and several intermetallic compounds. The maximum compressive fracture strengths at 20 °C of both alloys exceeded 620 MPa, while the compressive yield strengths at 300 °C were found to be >200 MPa; these values are two to three times higher than those of conventional Al alloys. The strengthening mechanism was mainly arising from solid solution hardening and intermetallic network hardening. After the thermal exposure at 300 °C for 100 h, an obvious change in appearance and composition of the high Mg-Zn containing phase occurred in  $\text{Al}_{74}\text{Cu}_{16}\text{Cr}_1\text{Zn}_7\text{Mg}_2$  alloy, which deteriorated the yield strength at 300 °C. In contrast, the  $\text{Al}_{78}\text{Cu}_{18}\text{Cr}_2\text{Zn}_1\text{V}_1$  alloy exhibited barely changed yield strength at 300 °C with a value of as high as 201 MPa after the thermal exposure, indicating its excellent thermal stability and great potential for high-temperature applications.

**Keywords:** Aluminum-based entropic alloys · Intermetallic network · Compressive properties · Thermal stability

## 1 Introduction

Traditional aluminum alloys are based on one principal element with the minor addition of alloying elements to obtain desirable mechanical and material properties. This conventional strategy limits the possibilities for full-range alloy development. In 2004, a brand-new classification of alloys named high-entropy alloys (HEAs) was developed by Yeh et al. [1] and Cantor et al. [2]. HEAs are equiatomic multicomponent alloys that include five or more equimolar or near-equimolar elements, thereby, improving the entropy of alloys and promoting the formation of solid solution phases. Many works have been devoted to developing various HEAs with simple phase formation and excellent properties [3]. Hereafter, using the concept of entropy, studies have been gradually

extended to new alloys named complex concentrated alloys, complex multicomponent alloys, entropic alloys, etc. [4].

Developing lightweight and low-cost structural alloys with outstanding high-temperature performance has attracted a great attention in recent years. Lightweight entropic alloys with a vast alloy design space have offered researchers' new avenues to explore novel materials. Many investigators have studied lightweight entropic alloys [5], and aluminum becomes the first choice of necessary elements. Due to the big difference in chemical properties among light elements, the lightweight entropic alloys usually have a more complex phase constitution than the high-entropy alloys [5]. Nevertheless, excellent mechanical properties such as high strength and good plasticity were achieved in lightweight entropic alloys. The  $\text{Al}_{20}\text{Be}_{20}\text{Fe}_{10}\text{Si}_{15}\text{Ti}_{35}$  alloy, with a density of  $3.91 \text{ g/cm}^3$ , showed an extremely high hardness value of 911 HV [6]. The compressive strength of the  $\text{Al}_{80}\text{Li}_5\text{Mg}_5\text{Zn}_5\text{Cu}_5$  alloy reached 800 MPa, with a plastic strain up to 17% [7]. The  $\text{Al}_{80}\text{Zn}_{14}\text{Li}_2\text{Mg}_2\text{Cu}_2$  alloy exhibited high compressive strengths of more than 1 GPa and high plasticity of more than 20% [8]. However, until now there are scarce reports focusing on the elevated-temperature mechanical properties of Al-based lightweight entropic alloys and their thermal stability.

In this study, two Al-based lightweight entropic alloys,  $\text{Al}_{74}\text{Cu}_{16}\text{Cr}_1\text{Zn}_7\text{Mg}_2$  and  $\text{Al}_{78}\text{Cu}_{18}\text{Cr}_2\text{Zn}_1\text{V}_1$ , were designed and studied. The microstructure characteristics, phase formation, and mechanical behavior at room and elevated temperatures were investigated. In addition, the thermal stability of the alloys was verified by prolonged thermal exposure at elevated temperature. Differences of the mechanical behavior between two alloys are elucidated, and the mechanism behind is discussed herein.

## 2 Experimental Procedure

In the alloy design of Al-based entropic alloys, Thermo-Calc software and TCAL7 database were used to calculate the equilibrium phases as a function of temperature. Cu was selected to form eutectic microstructure with Al in the alloys, because the eutectic microstructure can help improve the castability that is relatively poor in most entropic alloys [9, 10]. The type and proportion of elements were adjusted based on the physical thermodynamic parameters, e.g., mixing entropy and mixing enthalpy [11]. In the present study, two alloys,  $\text{Al}_{74}\text{Cu}_{16}\text{Cr}_1\text{Zn}_7\text{Mg}_2$  (Alloy-1) and  $\text{Al}_{78}\text{Cu}_{18}\text{Cr}_2\text{Zn}_1\text{V}_1$  (Alloy-2), were designed and investigated. They were melted in an induction melting furnace under an argon atmosphere and cast into a permanent copper mold. To ensure the chemical homogeneity, each ingot was remelted at least three times.

The microstructure of the alloys was examined by an optical microscope (OM, Nikon Eclipse ME600) and a scanning electron microscope (SEM, JEOL JSM-6480LV) equipped with an energy dispersive X-ray spectrometer (EDS). The phase identification was performed by an X-ray diffractometer (XRD, D8 Discover) using  $\text{Cu K}\alpha$  radiation, with a diffraction angle ( $2\theta$ ) range from  $10^\circ$  to  $80^\circ$ , a step size of  $0.05^\circ$ , and a step time of 0.5 s/step.

The mechanical properties were studied at room temperature (RT) and  $300^\circ\text{C}$  by conducting compression tests in a Gleeble 3800 thermomechanical simulator unit.

Cylindrical samples were used for the compression tests with a diameter of 8 mm and length of 12 mm. A part of the as-cast samples was thermally exposed at 300 °C for 100 h. At least two samples at the same condition were tested to verify the repeatability of the results.

### 3 Results and Discussion

#### 3.1 Predicted Phase Formation of the Alloys

According to the simulation of Thermo-Calc in Fig. 1, Alloy-1 consisted of five different phases. Al<sub>2</sub>Cu was the main phase, followed by fcc-Al. Al<sub>45</sub>Cr<sub>7</sub> was predicted to form at 600 °C and remain stable afterward. Two kinds of Mg-Zn phases (Mg<sub>2</sub>Zn<sub>11</sub> and MgZn<sub>2</sub>) also appeared. The predicted phases in Alloy-2 were simpler than in Alloy-1. Al<sub>2</sub>Cu was the predominant phase, followed by fcc-Al, Al<sub>45</sub>Cr<sub>7</sub>, and a very small amount of hcp-Zn. The Thermo-Calc simulation indicated a multicomponent microstructure of both alloys.

#### 3.2 As-Cast Microstructure and Phase Constituents

The XRD patterns of as-cast Alloy-1 and Alloy-2 were very similar, as shown in Fig. 2. Only three kinds of phases were detected, which were indexed as Al<sub>2</sub>Cu, fcc-Al, and Al<sub>45</sub>Cr<sub>7</sub>, respectively. These three phases were the most abundant phases in both alloys predicted by Thermo-Calc in Fig. 1. According to the intensity of the diffraction peak, Al<sub>2</sub>Cu was the major phase, followed by fcc-Al, then Al<sub>45</sub>Cr<sub>7</sub>, which is in accordance with the simulation results in Fig. 1. The alloys also contained other minor phases,

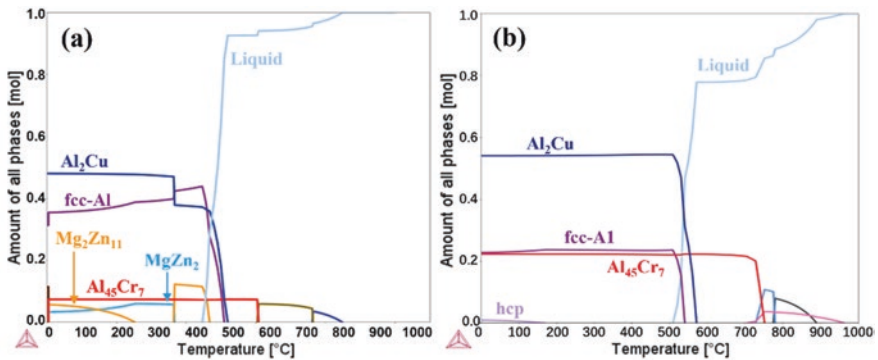


Fig. 1. Phase predictions of the two designed alloys calculated by Thermo-Calc: (a) Alloy-1 (Al<sub>74</sub>Cu<sub>16</sub>Cr<sub>1</sub>Zn<sub>7</sub>Mg<sub>2</sub>), (b) Alloy-2 (Al<sub>78</sub>Cu<sub>18</sub>Cr<sub>2</sub>Zn<sub>1</sub>V<sub>1</sub>).

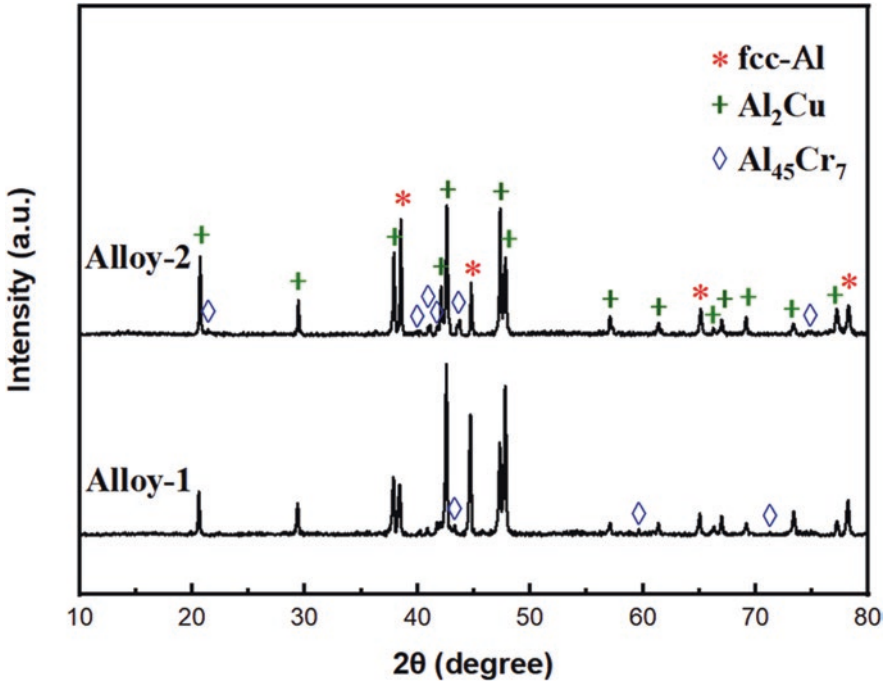


Fig. 2. XRD patterns of the as-cast Alloy-1 and Alloy-2.

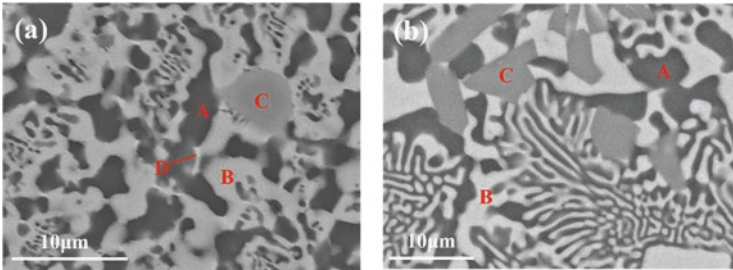


Fig. 3. SEM images of as-cast microstructure, (a) Alloy-1 and (b) Alloy-2.

which were not detected by XRD due to the low content. Therefore, SEM was further used to characterize the phase features.

Figure 3 showed the as-cast microstructure of two alloys. Based on morphology and brightness, four kinds of phases were identified in as-cast Alloy-1 in Fig. 3a, denoted as A, B, C, and D, respectively. According to the SEM-EDS results listed in Table 1, phase A contained 90 at.% Al, 5 at.% Cu, 3 at.% Zn, and 2 at.% Mg, which was determined as the fcc-Al matrix. The high content of Cu, Zn, and Mg in the matrix indicates a high solid solution. Correspondingly, phases B and C were identified as  $Al_2Cu$  and  $Al_{45}Cr_7$ . At the same time, a very small amount of phase D was detected, which contained simi-

**Table 1.** Chemical composition and volume fraction of different phases in the as-cast alloys.

Alloy	Density (g/cm <sup>3</sup> )	Region in Fig. 3	Chemical composition (at.%)						Phase name	Volume fraction (vol.%)
			Al	Cu	Cr	Zn	Mg	V		
Alloy-1	3.75	A	90	5	–	3	2	–	fcc-Al	33.45
		B	70	29	–	1	–	–	Al <sub>2</sub> Cu	58.33
		C	79	9	10	2	–	–	Al <sub>45</sub> Cr <sub>7</sub>	7.67
		D	74	15	–	5	6	–	Mg-Zn	0.55
Alloy-2	3.73	A	95	4	–	1	–	–	fcc-Al	30.11
		B	69	31	–	–	–	–	Al <sub>2</sub> Cu	54.53
		C	82	5	8	1	–	4	Al <sub>45</sub> Cr <sub>7</sub>	15.36

lar amount of Zn and Mg content. The volume fraction of each phase was quantified by image analyzing on at least 5 OM images. It can be found that phase D in Alloy-1 only took up 0.55 vol.%, much less than either of the MgZn<sub>2</sub> or Mg<sub>2</sub>Zn<sub>11</sub> predicted in Fig. 1, which could not be detected by XRD. Therefore, the phase D was temporarily referred as Mg-Zn in this work.

As-cast Alloy-2 in Fig. 3b contained three phases, dark phase A – fcc-Al, bright phase B – Al<sub>2</sub>Cu, and gray phase C – Al<sub>45</sub>Cr<sub>7</sub>. Compared with Alloy-1, Alloy-2 showed a more obvious eutectic microstructure consisting of fcc-Al and Al<sub>2</sub>Cu. The content of Al<sub>45</sub>Cr<sub>7</sub> in Alloy-2 was 15.36 vol.%, higher than that in Alloy-1 (7.67 vol.%), which was well supported by the Thermo-Calc simulation in Fig. 1.

From Table 1, both Alloy-1 and Alloy-2 were composed of the three main phases: Al<sub>2</sub>Cu followed by fcc-Al and Al<sub>45</sub>Cr<sub>7</sub>. And both alloys showed a lightweight property, with a low density of 3.75 and 3.73 g/cm<sup>3</sup>, respectively. It is apparent that results of Thermo-Calc simulation, XRD pattern, and SEM were comparable and supportive to each other.

### 3.3 Mechanical Properties and Thermal Stability

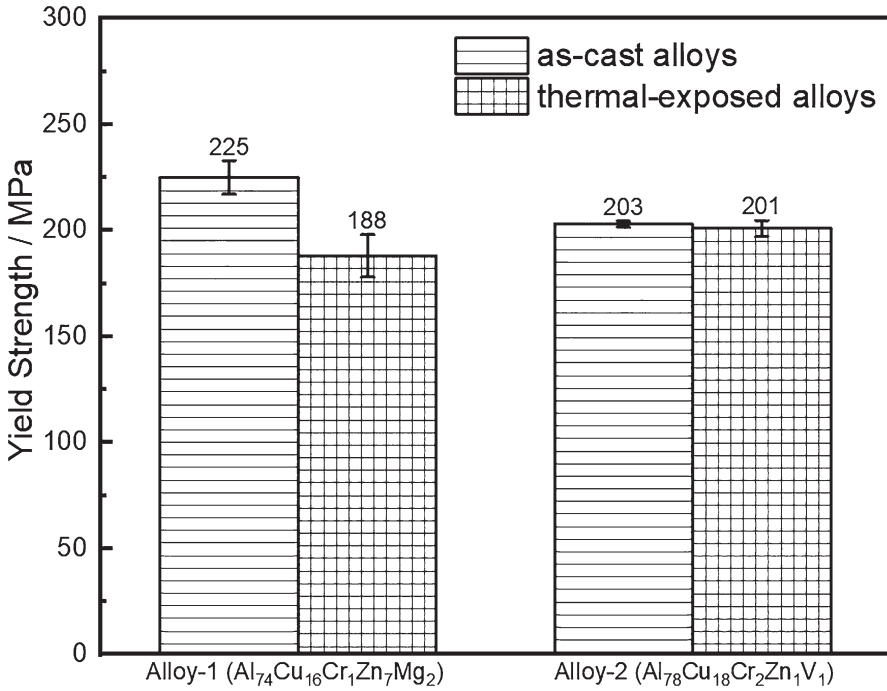
Compression tests of as-cast Alloy-1 and Alloy-2 were first conducted at room temperature, and the results are listed in Table 2. Alloy-1 and Alloy-2 exhibited a yield strength (YS)  $\sigma_{0.2}$  of 588 and 387 MPa, respectively. Alloy-1 and Alloy-2 displayed similar fracture strength  $\sigma_{max}$  of 624 and 621 MPa, which are 2–3 times higher than that of conventional Al cast alloys. The low-fracture strain  $\epsilon_p$  of both alloys indicates a poor ductility. The high strengths of as-cast Alloy-1 and Alloy-2 can be attributed to two reasons: one is the high solid solution (SS) strengthening, and the other is the strong intermetallic (IC) network in the two alloys. The large difference between YS values of the two alloys can be ascribed to the different SS strengthening and distinct IC network in the two alloys.

The SS strengthening ( $\Delta\sigma_{SS}$ ) at room temperature can be calculated according to the following equation [12, 13]

$$\Delta\sigma_{SS} = HC^\alpha, \quad (1)$$

**Table 2.** Compressive mechanical properties of the as-cast alloys.

Alloy	$\sigma_{0.2}$ (MPa)	$\sigma_{\max}$ (MPa)	$\epsilon_p$ (%)
Alloy-1	588	624	0.72
Alloy-2	387	621	1.05

**Fig. 4.** Yield strength of as-cast alloys and thermal-exposed alloys at 300 °C.

wherein  $C$  is the concentration of solute atoms, and  $H$  and  $\alpha$  are positive constants for a certain element. From Table 1, Alloy-1 contained more Cu, Zn, and Mg solute atoms in fcc-Al matrix than Alloy-2 did. Therefore, the solid solution strengthening of Alloy-1 was higher than Alloy-2. In addition, Al<sub>2</sub>Cu in Alloy-1 was mainly in compact block form, compared with the thin lamellar Al<sub>2</sub>Cu in Alloy-2, and the compact block form of Al<sub>2</sub>Cu in Alloy-1 made the IC network stronger. It is reported that the block ICs are typically the source of cracking [14]. Therefore, Alloy-1 showed a lower  $\epsilon_p$  than Alloy-2.

To study the mechanical properties of the alloys at high temperature, compression tests of the as-cast alloys were conducted at 300 °C and the results are shown in Fig. 4. The YS values of both as-cast alloys at 300 °C exceeded 200 MPa, showing excellent mechanical strength at high temperature. It is reported that Al<sub>2</sub>Cu and Al<sub>45</sub>Cr<sub>7</sub> can be present at high temperature up to 520 °C [15]. The chemical composition of Al<sub>2</sub>Cu and Al<sub>45</sub>Cr<sub>7</sub> in the alloys after being exposed at 300 °C was checked by EDS, and it showed

the same results as listed in Table 1, which confirmed the stability of these two ICs. Therefore, the high YSs, which far exceeded that of commercial Al cast alloys, was believed largely due to the high contribution of the strong IC networks of  $\text{Al}_2\text{Cu}$  and  $\text{Al}_{45}\text{Cr}_7$  at 300 °C.

In addition to elevated-temperature YS, the thermal stability is one important aspect of the alloy applicable at elevated temperature. Thermal exposure experiment was carried out to the as-cast alloys at 300 °C for 100 h, followed by the compression test at 300 °C, and the results are shown in Fig. 4. Alloy-2 exhibited a high YS of 201 MPa after thermal exposure, which was barely changed compared with the as-cast alloy, indicating its excellent thermal stability. However, Alloy-1 showed a low YS of 188 MPa, deceased largely from the YS at as-cast condition (225 MPa). To explore the mechanism behind, the microstructure of thermal-exposed alloys was further observed, as shown in Fig. 5.

OM images of Fig. 5 showed the microstructure after thermal exposure for both alloys. Compared with the as-cast alloys whose OM images are embedded in the top-right corners of Fig. 5a and b, a “new” phase E occurred in Alloy-1 after thermal exposure (white arrows in Fig. 5a), while the main phases in thermal-exposed Alloy-2 remained unchanged and they exhibited the same chemical composition as the as-cast alloy as indicated by EDS results. The “new” phase E in Alloy-1 had a volume fraction of 2.6 vol.%, larger than phase D in the as-cast alloy. Moreover, it can be found that phase E always existed around  $\text{Al}_2\text{Cu}$ . Phase E displayed a bright color under backscatter SEM mode (red arrows in Fig. 6), and the SEM-EDS result also revealed that phase E had a high content of Zn and Mg, especially Zn, much higher than phase D in Table 1. In addition, the  $\text{Al}_2\text{Cu}$  phase in as-cast Alloy-1 contained Zn (1 at.%), while no Zn was detected in the  $\text{Al}_2\text{Cu}$  of thermal-exposed Alloy-1, indicating the Zn diffusion from  $\text{Al}_2\text{Cu}$  to phase E. In the meantime, Mg was barely detected in the matrix in the thermal-exposed Alloy-1, which also diffused to the phase E. Phase E may be a result of phase transformation from phase D, according to the Thermo-Calc simulation in Fig. 1, a phase transformation from  $\text{MgZn}_2$  to  $\text{Mg}_2\text{Zn}_{11}$  may occur after a long thermal exposure at 300 °C; on the other side, phase E may just be the product of a change in the chemical composition of phase D. Either of them indicates the poor thermal stability of the high Mg-Zn containing phase D. Further experiments regarding this transformation, either

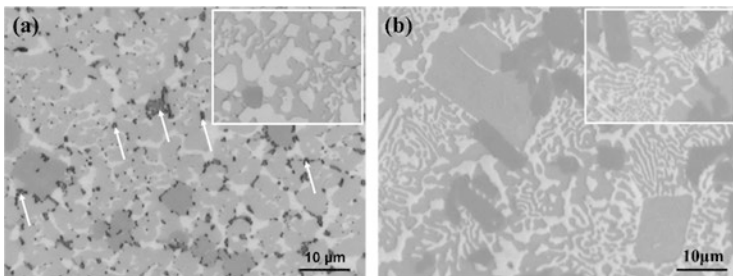


**Fig. 5.** OM images after thermal exposure at 300 °C for 100 h, (a) Alloy-1 and (b) Alloy-2.

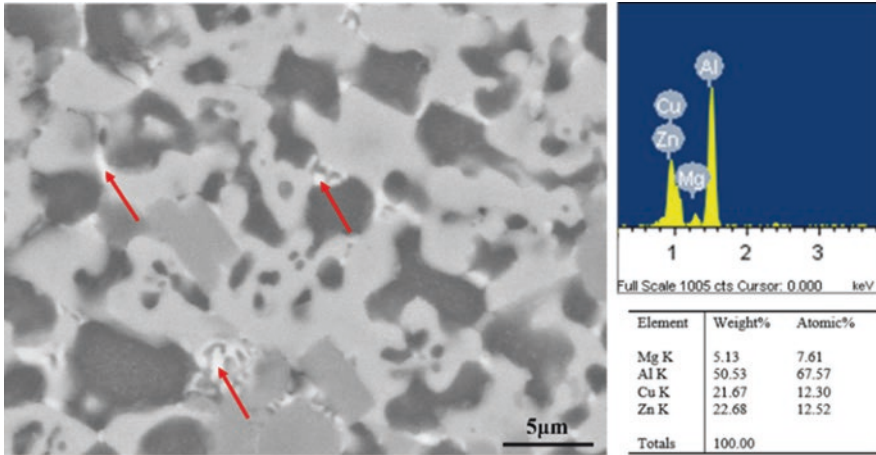


Fig. 6. SEM-EDS of thermal-exposed Alloy-1.

chemical compositionally or crystal structurally, will be conducted to give hints to future research on the development of lightweight entropic alloys.

Phase E mainly located in the interfaces between  $\text{Al}_2\text{Cu}$  and fcc-Al, which might weak the original strong IC network structure. According to SEM-EDS results, Mg and Zn solute atoms in the fcc-Al matrix partially diffused to phase E after thermal exposure, causing a decrease of the SS strengthening in the matrix. These two factors resulted in a big drop-off in YS of Alloy-1 after thermal exposure. Meanwhile, the main phases in Alloy-2 were thermally stable, ensuring its high YS after thermal exposure. This suggests that the simultaneous addition of Mg and Zn with a high content induced an unsatisfactory high-temperature property and a low thermal stability, which should be avoided in the lightweight entropic alloys for applications at elevated temperature.

To compare the elevated-temperature strength of different Al alloys, a parameter  $R$  is introduced in this work:

$$R = \frac{\sigma_{0.2}}{\rho}, \quad (2)$$

wherein  $\sigma_{0.2}$  is the yield strength at 300 °C of alloys at the thermal exposure condition of 300 °C/100 h, and  $\rho$  is the alloy density either published or estimated by chemical composition [16]. It can be seen that with a certain limitation of the alloy density (for example, 4.5 g/cm<sup>3</sup>) [17], the larger the  $R$  value is, the more the alloy conforms to the lightweight and high strength, and the greater the potential of its application at elevated temperature in the transportation (automobile and aerospace) industries.

Recently, several studies have been focused on the improvements of elevated-temperature mechanical properties and the thermal stability of Al alloys [18–23]. Figure 7 shows the comparison of the  $R$  value and YS value of several laboratory improved Al alloys with Alloy-1 and Alloy-2 in the present work. For example, the heat treatment improved 3004 alloy exhibited a YS of 78 MPa and a  $R$  value of 29 kN·m/kg



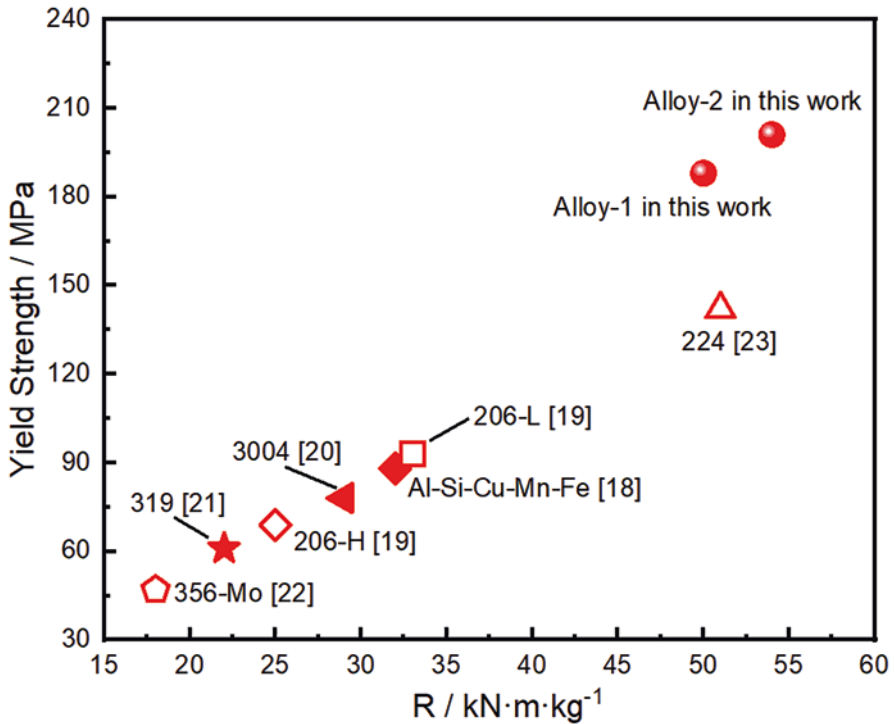


Fig. 7. Yield strength at 300 °C after thermal exposure of 300 °C/100 h vs  $R$  of the alloys in this work and several Al alloys in references.

after thermal exposure at 300 °C/100 h [20], the modified low Si/Mn concentration 206-L alloy had a YS of 93 MPa and a  $R$  value of 33 kN·m/kg [19], and the Mg-micro alloyed 224 alloy displayed a high yield strength of 142 MPa and a good  $R$  of 51 kN·m/kg [23]. Alloy-2 in this work showed a YS up to 201 MPa as well as a high  $R$  of 54 kN·m/kg, indicating its beneficial potential for applications at high temperatures.

## 4 Conclusions

1. Two Al-based lightweight entropic alloys,  $\text{Al}_{74}\text{Cu}_{16}\text{Cr}_1\text{Zn}_7\text{Mg}_2$  and  $\text{Al}_{78}\text{Cu}_{18}\text{Cr}_2\text{Zn}_1\text{V}_1$ , were designed and studied in this work. The as-cast microstructure of the two entropic alloys revealed a multiphase feature. The phase prediction of the Thermo-Calc simulation was in good agreement with XRD and metallographic results.
2.  $\text{Al}_{74}\text{Cu}_{16}\text{Cr}_1\text{Zn}_7\text{Mg}_2$  and  $\text{Al}_{78}\text{Cu}_{18}\text{Cr}_2\text{Zn}_1\text{V}_1$  alloys showed YS values of 588 MPa and 387 MPa at room temperature, and high YS values of more than 200 MPa at 300 °C, respectively. The strengthening of both alloys was mainly contributed by the solid solution strengthening and the intermetallic network hardening.

3. After thermal exposure at 300 °C for 100 h, the YS at 300 °C of  $\text{Al}_{7.4}\text{Cu}_{1.6}\text{Cr}_1\text{Zn}_7\text{Mg}_2$  alloys deteriorated from 225 to 188 MPa, owing to the decreased SS strengthening in the matrix as well as the poor thermal stability of the high Mg-Zn containing phase. Therefore, the simultaneous addition of Mg and Zn with a high content is not recommended in the lightweight entropic alloys for applications at elevated temperature.
4. Compared with the as-cast alloy, the thermal-exposed  $\text{Al}_{7.8}\text{Cu}_{1.8}\text{Cr}_2\text{Zn}_1\text{V}_1$  alloy showed a barely changed YS of 201 MPa at 300 °C, indicating its excellent thermal stability due to the heat resistance of the main phases. Although the alloy density of  $\text{Al}_{7.8}\text{Cu}_{1.8}\text{Cr}_2\text{Zn}_1\text{V}_1$  is moderately higher than conventional Al alloy, the high  $R$  value of this alloy suggests its great potential for applications at high temperature.

**Acknowledgments** The authors gratefully acknowledge the financial support of the Natural Sciences and Engineering Research Council of Canada (NSERC) under the Grant No. CRDPJ 514651-17 and Rio Tinto Aluminum through the Research Chair in the Metallurgy of Aluminum Transformation at University of Quebec at Chicoutimi.

## References

1. Yeh JW, Chen SK, Lin SJ, et al. Nanostructured high-entropy alloys with multiple principal elements: novel alloy design concepts and outcomes. *Adv Eng Mater.* 2004;6:299–303. <https://doi.org/10.1002/adem.200300567>.
2. Cantor B, Chang ITH, Knight P, et al. Microstructural development in equiatomic multicomponent alloys. *Mater Sci Eng A.* 2004;375:213–8. <https://doi.org/10.1016/j.msea.2003.10.257>.
3. Zhang Y, Zuo TT, Tang Z, et al. Microstructures and properties of high-entropy alloys. *Prog Mater Sci.* 2014;61:1–93. <https://doi.org/10.1016/j.pmatsci.2013.10.001>.
4. Miracle DB, Senkov ON. A critical review of high entropy alloys and related concepts. *Acta Mater.* 2017;122:448–511. <https://doi.org/10.1016/j.actamat.2016.08.081>.
5. Li Y, Zhang Y. Light-weight and flexible high-entropy alloys. In: Sharma A, Duriagina Z, Kumar S, editors. *Engineering steels and high entropy-alloys*. London: IntechOpen; 2019. <https://doi.org/10.5772/intechopen.88332>.
6. Tseng K, Yang Y, Juan C, et al. A light-weight high-entropy alloy  $\text{Al}_{20}\text{Be}_{20}\text{Fe}_{10}\text{Si}_{15}\text{Ti}_{35}$ . *Sci China Technol Sci.* 2018;61:184–8. <https://doi.org/10.1007/s11431-017-9073-0>.
7. Yang X, Chen SY, Cotton JD, et al. Phase stability of low-density, multiprincipal component alloys containing aluminum, magnesium, and lithium. *JOM.* 2014;66:2009–20. <https://doi.org/10.1007/s11837-014-1059-z>.
8. Li R, Ren Z, Wu Y, et al. Mechanical behaviors and precipitation transformation of the light-weight high-Zn-content  $\text{Al-Zn-Li-Mg-Cu}$  alloy. *Mater Sci Eng A.* 2021;802:140637. <https://doi.org/10.1016/j.msea.2020.140637>.
9. Lu Y, Gao X, Jiang L, et al. Directly cast bulk eutectic and near-eutectic high entropy alloys with balanced strength and ductility in a wide temperature range. *Acta Mater.* 2017;124:143–50. <https://doi.org/10.1016/j.actamat.2016.11.016>.
10. Shao L, Zhang T, Li L, et al. A low-cost lightweight entropic alloy with high strength. *J Mater Eng Perform.* 2018;27:6648–56. <https://doi.org/10.1007/s11665-018-3720-0>.
11. Zhang Y, Yang X, Liaw PK. Alloy design and properties optimization of high-entropy alloys. *JOM.* 2012;64:830–8. <https://doi.org/10.1007/s11837-012-0366-5>.
12. Ryen Ø, Holmedal B, Nijs O, et al. Strengthening mechanisms in solid solution aluminum alloys. *Metall Mater Trans A Phys Metall Mater Sci.* 2006;37:1999–2006. <https://doi.org/10.1007/s11661-006-0142-7>.

13. Li Z, Zhang Z, Chen XG. Improvement in the mechanical properties and creep resistance of Al-Mn-Mg 3004 alloy with Sc and Zr addition. *Mater Sci Eng A*. 2018;729:196–207. <https://doi.org/10.1016/j.msea.2018.05.055>.
14. Singh SS, Guo E, Xie H, et al. Mechanical properties of intermetallic inclusions in Al 7075 alloys by micropillar compression. *Intermetallics*. 2015;62:69–75. <https://doi.org/10.1016/j.intermet.2015.03.008>.
15. Glazoff MV, Khvan A, Zolotarevsky VS, et al. *Casting aluminum alloys: their physical and mechanical metallurgy*. 2nd ed. Butterworth-Heinemann; 2018.
16. Chauhan P, Yebaji S, Nadakuduru VN, et al. Development of a novel light weight Al35Cr14Mg6Ti35V10 high entropy alloy using mechanical alloying and spark plasma sintering. *J Alloys Compd*. 2020;820:153367. <https://doi.org/10.1016/j.jallcom.2019.153367>.
17. Campbell FC. *Lightweight materials: understanding the basics*, 4. ASM International; 2012. <https://doi.org/10.31399/asm.tb.lmub.t53550001>.
18. Lin B, Li H, Xu R, et al. Thermal exposure of Al-Si-Cu-Mn-Fe alloys and its contribution to high temperature mechanical properties. *J Mater Res Technol*. 2020;9:1856–65. <https://doi.org/10.1016/j.jmrt.2019.12.018>.
19. Rakhmonov J, Liu K, Chen GX. Effects of compositional variation on the thermal stability of  $\theta'$ -Al<sub>2</sub>Cu precipitates and elevated-temperature strengths in Al-Cu 206 alloys. *J Mater Eng Perform*. 2020;29:7221–30. <https://doi.org/10.1007/s11665-020-05227-5>.
20. Liu K, Chen XG. Development of Al-Mn-Mg 3004 alloy for applications at elevated temperature via dispersoid strengthening. *Mater Des*. 2015;84:340–50. <https://doi.org/10.1016/j.matdes.2015.06.140>.
21. Jin L, Liu K, Chen XG. Evolution of dispersoids and their effects on elevated-temperature strength and creep resistance in Al-Si-Cu 319 cast alloys with Mn and Mo additions. *Mater Sci Eng A*. 2020;770:138554. <https://doi.org/10.1016/j.msea.2019.138554>.
22. Farkoosh AR, Chen XG, Pekguleryuz M. Dispersoid strengthening of a high temperature Al-Si-Cu-Mg alloy via Mo addition. *Mater Sci Eng A*. 2015;620:181–9. <https://doi.org/10.1016/j.msea.2014.10.004>.
23. Rakhmonov J, Liu K, Pan L, et al. Enhanced mechanical properties of high-temperature-resistant Al-Cu cast alloy by microalloying with Mg. *J Alloys Compd*. 2020;827:154305. <https://doi.org/10.1016/j.jallcom.2020.154305>.